ISSN 1849-0700
ISSN 1330-0083
CODEN HMCAE7

Hrvatsko meteorološko društvo
Croatian Meteorological Society

HRVATSKI METEOROLOŠKI ČASOPIS
CROATIAN METEOROLOGICAL JOURNAL

56

Hrv. meteor. časopis	Vol. 56	p. 1-216	ZAGREB	2023

HRVATSKI METEOROLOŠKI ČASOPIS
CROATIAN METEOROLOGICAL JOURNAL

Izdaje
Hrvatsko meteorološko društvo
Ravnice 48, 10000 Zagreb
Hrvatska

Published by
Croatian Meteorological Society
Ravnice 48, 10000 Zagreb
Croatia

Glavna i odgovorna urednica / Chief Editor
Tanja Likso, Zagreb hmc@meteohmd.hr
Zamjenik glavne i odgovorne urednice / Assistant Editor
Krešo Pandžić, Zagreb

Tajnica / Secretary
Ljilja Ivušić, Zagreb ljiljaivusic@gmail.com

Urednički odbor / Editorial board
Tanja Likso, Zagreb
Goran Gašparac, Zagreb
Antun Marki, Zagreb
Vinko Šoljan, Split
Ljilja Ivušić, Zagreb
Krešo Pandžić, Zagreb
Branko Grisogono, Zagreb
Katarina Stanković, Zagreb
Ivan Toman, Zadar

Recenzenti / Reviewers
Simon Berkowicz, Izrael
Kristan Horvath, Hrvatska
Jadran Jurković, Hrvatska
Giora Kidron, Izrael
Tanja Likso, Hrvatska
Renata Sokol Jurković, Hrvatska
Ivana Tošić, Srbija
Ksenija Zaninović, Hrvatska
Vesna Đuričić, Hrvatska
Branka Ivančan-Picek, Hrvatska
Ján Kaňák, Slovačka
Gabin Koto N'Gobi, Bénin
Krešo Pandžić, Hrvatska
Lidija Srnec, Hrvatska
Josip Vuković, Hrvatska

Lektura / Proofreading
Neoplazam (hrv.), Alpha (eng.)

Korektura / Corrections
Vesna Đuričić, Hrvatska

Časopis se referira u / Abstracted in
Scopus
Geobase
Elsevier/Geoabstracts
Zugänge der Bibliotheke des Deutschen Wetterdienstes
Meteorological and Geoastrophysical Abstracts
Abstracts Journal VINITI

Adrese za slanje radova / Addresses for papers acceptance
hmc@meteohmd.hr
likso@cirus.dhz.hr

Časopis izlazi godišnje
Web izdanje: *http://hrcak.srce.hr/hmc*
Prijelom i tisak: ABS 95

Naklada: 150 primjeraka

Hrvatsko meteorološko društvo
Croatian Meteorological Society

HRVATSKI METEOROLOŠKI ČASOPIS
CROATIAN METEOROLOGICAL JOURNAL

56

Hrv. meteor. časopis	Vol. 56	p. 1-216	ZAGREB	2023

Znanstveni časopis *Hrvatski meteorološki časopis* nastavak je znanstvenog časopisa *Rasprave* koji redovito izlazi od 1982. godine do kada je časopis bio stručni pod nazivom *Rasprave i prikazi* (osnovan 1957.). U časopisu se objavljuju znanstveni i stručni radovi iz područja meteorologije i srodnih znanosti. Objavom rada u Hrvatskom meteorološkom časopisu autori se slažu da se rad objavi na internetskim portalima znanstvenih časopisa, uz poštivanje autorskih prava

Scientific journal *Croatian Meteorological Journal* succeeds the scientific journal *Rasprave,* which has been published regularly since 1982. Before the year 1982 journal had been published as professional one under the title *Rasprave i prikazi* (established in 1957). The *Croatian Meteorological Journal* publishes scientific and professional papers in the field of meteorology and related sciences.
Authors agree that articles will be published on internet portals of scientific magazines with respect to author's rights.

Hrvatski meteorološki časopis – Croatian Meteorological Journal, 56, 2023, 17–29
https://doi.org/10.37982/hmc.56.1.2

Izvorni znanstveni rad
Original scientific paper

DEVELOPMENT OF BI-NORMALIZED BURN RATIO METHOD ON THE CATASTROPHIC FOREST FIRE EVENT 14TH JULY 2022 NEAR VODICE, CROATIA

Razvoj metode bi-normaliziranog omjera opožarenosti na događaju katastrofalnog šumskog požara 14. srpnja 2022. kod Vodica, Hrvatska

MLADEN VIHER[1], BERNARDA KRULIĆ MUTAVČIĆ[2]
and VALNEA KERBAVČIĆ DEGAČ[3]

[1] Croatian Military Academy "Dr. Franjo Tuđman"
Ilica 256b, 10000 Zagreb, Croatia
[2]General Staff of the Armed Forces of the Republic of Croatia,
Control Operational Centre
Krešimirov trg 1, 10000 Zagreb, Croatia
[3]Ministry of Defence, Real Estate and Environmental Protection Department,
GIS and Meteorology Division
Krešimirov trg 1, 10000 Zagreb, Croatia
mviher@unizg.hr

Received 27 August 2022, in final form 26 March 2023
Primljeno 27. kolovoza 2022., u konačnom obliku 26. ožujka 2023.

Abstract: The use of multispectral sensors, such as MSI, on the Sentinel-2 satellite for rapid assessment of the area and the burning degree after large forest fires utilises standard method of determining the Normalized Burn Ratio (NBR) before and after the fire, from which the difference of the Normalized Burn Ratio (dNBR) is calculated. Applied to areas with sparse vegetation, the standard method of NBR gives poor results. To cope with low vegetation areas, a so-called "relativizing dNBR" was introduced where an empirical expression divides the difference of the NBRs in two channels by a quotient slightly greater than the pre-fire NBR.
In this paper, a forest fire near Vodice, Croatia, which occurred on July 14, 2022, and which grew into a catastrophic fire that left about 30 km^2 of burnt area, was studied. As this is an area of Mediterranean vegetation, relatively sparse, instead of the relativization, an attempt was made to introduce a new formula for calculating the normalized ratio of burning, which included two differences in spectral radiances (instead of one). In addition to the standard difference in the near-infrared and short-wave infrared part of the spectrum, a difference between the near-infrared and the green visible part of the spectrum was used simultaneously. These new, bi-Normalized Burn Ratio, retain information about the spectral radiance in the green visible band and react to surfaces where at least a little vegetation cover remained after the fire, which ultimately gives lower burn categories, with the same burned area detected compared to the standard method.

Key words: remote sensing, forest fires, Normalized Burn Ratio (NBR), multispectral sensor

Sažetak: Multispektralni senzori, poput MSI-ja na satelitu Sentinel-2 za brzu procjenu površine i stupnja opožarenosti nakon velikih šumskih požara koriste se standardnom metodom određivanja normaliziranog omjera opožarenosti (NBR) prije i poslije požara, iz kojih se računa razlika normaliziranog omjera opožarenosti (dNBR). Standardna metoda ima nedostatak kad se primjenjuje na površinama s rijetkom vegetacijom te se preporučuje tzv. relativiziranje dNBR empiričkim izrazom koji dijeli razliku NBR-a s kvocijentom malo većim od NBR-a prije požara. U ovom radu proučen je šumski požar kod Vodica, Hrvatska, koji se dogodio 14. srpnja 2022. i koji je prerastao u katastrofalni požar nakon kojeg je ostalo oko 30 km^2 opožare-

nog područja. S obzirom na to da je to područje relativno rijetke mediteranske vegetacije, umjesto relativizacije pokušala se uvesti nova formula za računanje normaliziranog omjera opožarenosti koja je uključivala dvije razlike spektralnih radijanci; uz standardnu razliku u bliskom infracrvenom i kratkovalnom infracrvenom dijelu spektra uvedena je razlika između bliskog infracrvenog i zelenog vidljivog dijela spektra. Taj bi-normalizirani omjer opožarenosti zadržava informaciju o spektralnoj radijanci u zelenom vidljivom području te reagira na površine gdje je nakon požara preostalo barem malo vegetacijskog pokrova što naposljetku daje niže kategorije opožarenosti, uz istu detektiranu površinu opožarenosti u odnosu na standardnu metodu.

Ključne riječi: daljinska istraživanja, šumski požari, normalizirani omjer opožarenosti (NBR), multispektralni senzor

1. INTRODUCTION

Forest fires represent a real and great danger in the Republic of Croatia (Figs. 2 and 3), especially in its Coastal region. The immediate reason for writing this paper was the huge forest fire that occurred on 14th July 2022 near the coastal town Vodice, which burned 29 km^2 of land area and caused great material damage (Figs. 1, 1A, 1B and 2). The occurrence and causes of forest fires in Croatia have been analysed in detail: individual researchers (Jurjević et al., 2009), the Croatian Bureau of Statistics (https://podaci.dzs.hr/2021/hr/10149), Croatian Forests (https://www.hrsume.hr/index.php/hr/sume/zastita-suma-od-pozara) and

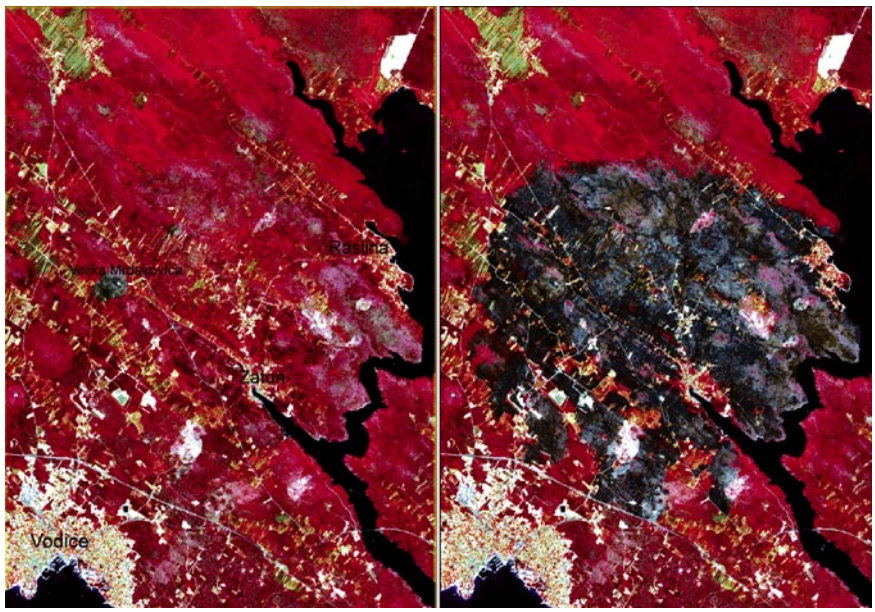

Figure 1. Sentinel-2B satellite images taken before the fire (left, taken on July the 6th, 2022) and immediately after the fire (right, taken on July the 16th, 2022) and shown as a standard photo in the near-infrared part of the spectrum as used in forestry where the vegetation is expressed through the intensity and saturation of the red colour - the image before the fire shows a scar from an earlier smaller fire near the Velika Mrdakovica hamlet, while the image on the right shows the consequences of the forest fire that broke out on July 14, 2022 and burned almost 30 km^2 of land areas.

Slika 1. Snimke sa satelita Sentinel-2B prije požara (lijevo, snimljeno 6. srpnja 2022.) i neposredno poslije požara (desno, snimljeno 16. srpnja 2022.) prikazane kao standardna fotografija u bliskom infracrvenom dijelu spektra kako se upotrebljava u šumarstvu na kojoj je vegetacija izražena intenzitetom i zasićenjem crvene boje – na snimci prije požara vidljiv je ožiljak od ranijeg manjeg požara kod zaselka Velika Mrdakovica, dok snimka desno pokazuje posljedice šumskog požara koji je izbio 14. srpnja 2022. i u kojem je opožareno gotovo 30 km^2 površine.

the Croatian Meteorological and Hydrological Service (https://meteo.hr/podaci.php?section=podaci_agro&param=pozarind). Forest fire statistics in the European Union are also dealt with by the European Forest Fire Information System (EFFIS), which issues technical reports on forest fires in European countries (San-Miguel-Ayanz et al., 2021), and on its website provides a comparative analysis of the number of fires and total burned areas (https://effis.jrc.ec.europa.eu/apps/effis.statistics/estimates) (Figs. 2 and 3) with interpretations (San-Miguel-Ayanz et al., 2020). A recent work (Vuković, 2020) emphasizes the great effort invested in the planning, implementation and analysis of the effectiveness of forest fire protection in the Republic of Croatia.

Figure 1a. The full Sentinel-2B scene acquired on 6th July 2022 starting at 09:50:39 UTC and finishing at 11:30:52 UTC, represented in visible part of spectrum (RGB = channels: 432); there are no cloud contamination over subset area near Vodice (Fig. 1), cumulimorphic clouds are present near Trogir and in the north-eastern part of the scene.

Slika 1a. Cijelo područje sa satelita Sentinel-2B snimljeno na dan 6. srpnja 2022. počevši u 09:50:39 UTC te završivši u 11:30:52 UTC, prikazano u vidljivom dijelu spektra (RGB = kanali: 432); smetnje od naoblake nisu bile prisutne u izdvojenom području oko Vodica (sl. 1), kumulimorfna naoblaka vidljiva je samo blizu Trogira te u sjeveroistočnom dijelu područja.

Figure 1b. The full Sentinel-2B scene acquired on 16th July 2022 starting at 09:45:49 UTC and finishing at 11:40:17 UTC, represented in visible part of spectrum (RGB = channels: 432); there are no cloud contamination over subset area near Vodice (Fig. 1), cumulimorphic clouds are in the northeastern part of the scene only.

Slika 1b. Cijelo područje sa satelita Sentinel-2B snimljeno na dan 16. srpnja 2022. počevši u 09:45:49 UTC te završivši u 11:40:17 UTC, prikazano u vidljivom dijelu spektra (RGB = kanali: 432); smetnje od naoblake nisu bile prisutne u izdvojenom području oko Vodica (sl. 1), kumulimorfna naoblaka vidljiva je samo u sjeveroistočnom dijelu područja.

The idea of this paper is the development of a method for a quick and precise assessment of the burned area with degrees of the burns in accordance with the EFFIS methodology (EFFIS, 2018). The method uses radiometric remote sensing from sensors on the Sentinel-2 satellite, from the Copernicus program of the European Union. For its application, two satellite images are required, immediately before and immediately after the fire, on which the normalized surface burn ratio (NBR) is calculated in the first step. In the second step, from the difference of the NBRs on both images, the differential normalized burn index (dNBR) is obtained which is graded according to the EFFIS methodology into five categories: non-burned, lightly burned, medium burned, heavily burned and very heavily burned areas. During processing, water surfaces that could affect the accuracy of the NBR calculation are extracted from the satellite images. Clouds have to be masked out too,

but both images in this work have no clouds contamination (Figs. 1A and 1B). At the end, the images are orthorectified using a digital terrain model and translated into a geographic projection and scale so that the amount of burnt area can be calculated.

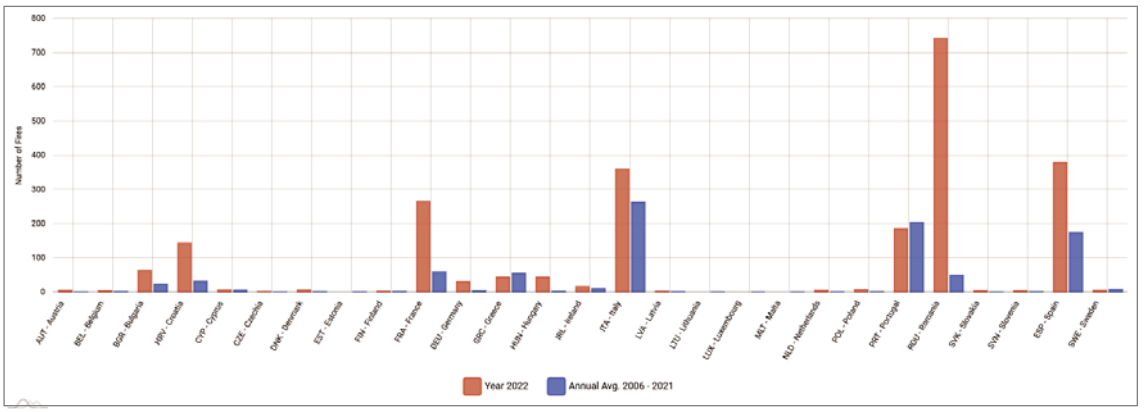

Figure 2. The average annual number of fires in the countries of the European Union compared to the current number of fires in 2022. By the time of writing this work (first half of August 2022), the Republic of Croatia is among the countries with the highest number of forest fires; the number of fires that occurred this year already exceeds the average annual number of fires. Source: https://effis.jrc.ec.europa.eu/apps/effis.statistics/estimates, reprinted according to the reuse policy of the EC, implemented by the Commission Decision 2011/833/EU of 12 December 2011 on the reuse of Commission documents (OJ L 330, 14.12.2011, p. 39).

Slika 2. Prosječan godišnji broj požara u zemljama Europske unije uspoređen s aktualnim brojem požara u 2022. godini do vremena pisanja članka (prva polovina kolovoza 2022.), Republika Hrvatska je među zemljama s najvećim brojem šumskih požara, s tim da broj požara ove godine već nadmašuje prosječan godišnji broj požara. Izvor: https://effis.jrc.ec.europa.eu/apps/effis.statistics/estimates, preneseno iz izvornika uz navođenje izvora, u skladu s politikom ponovnog korištenja implementiranom odlukom EC 2011/833/EU od 12. 12. 2011. o ponovnoj upotrebi dokumenata Komisije (OJ L 330, 14.12.2011, p. 39).

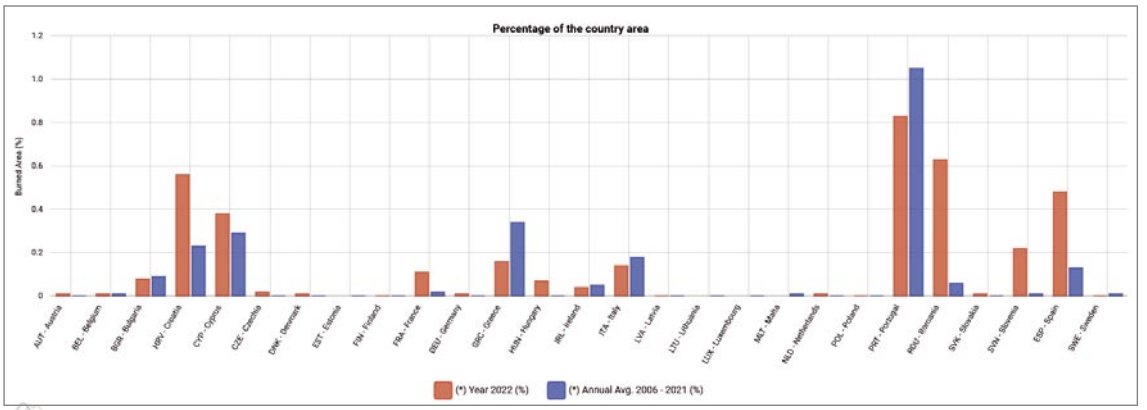

Figure 3. Burned area in proportion to the total area of the territory for the countries of the European Union, the average during the period 2006–2021 and the percentage of the burned territory in the current year until the time of writing of this work (the first half of August 2022), the Republic of Croatia is fourth in terms of the total burned area among EU countries during period 2006–2021 and third in percentage of the country burned area in the first half of 2022. Source: https://effis.jrc.ec.europa.eu/apps/effis.statistics/estimates, reprinted according to the reuse policy of the EC, implemented by the Commission Decision 2011/833/EU of 12 December 2011 on the reuse of Commission documents (OJ L 330, 14.12.2011, p. 39).

Slika 3. Opožarena površina u omjeru prema ukupnoj površini teritorija za zemlje Europske unije, prosjek u razdoblju 2006. – 2021. i postotak opožarenog teritorija u tekućoj godini do vremena pisanja članka (prva polovina kolovoza 2022.), Republika Hrvatska treća je po ukupnom opožarenom području u prvoj polovici 2022. te četvrta po postotku opožarene površine među zemljama EU u razdoblju 2006. – 2021. Izvor: https://effis.jrc.ec.europa.eu/apps/effis.statistics/estimates, preneseno iz izvornika uz navođenje izvora, u skladu s politikom ponovnog korištenja implementiranom odlukom EC 2011/833/EU od 12. 12. 2011. o ponovnoj upotrebi dokumenata Komisije (OJ L 330, 14.12.2011, p. 39).

2. METHODOLOGY

2.1. Spectral radiance

In the work, radiometric sensors on the Sentinel-2 satellite were used to measure the spectral radiance of reflected solar radiation from the surface in a narrow band of wavelengths. The satellite is placed in orbit so that the observed area always overflies at the same local time, so in the case of a small time difference between successive images, the radiometric conditions will be almost the same. Wavelengths used in this work have shorter wave lengths, dominated by reflected solar radiation for which, according to the radiation budget equation, the total amount of radiant flux Φ_T in specific spectral band $\Delta\lambda$ is (Campbell et al., 2022):

$$\Phi_T(\lambda) = \Phi_{reflected}(\lambda) + \Phi_{absorbed}(\lambda) + \Phi_{transmitted}(\lambda) \quad (1)$$

Only a part of the radiation flux that was reflected from the surface $\Phi(\lambda)$ will reach the satellite sensor, and its flow over the entire hemisphere is (Campbell et al., 2022):

$$\Phi(\lambda) = \int_{\lambda_1}^{\lambda_2} \Phi_{reflected}(\lambda) \cdot S(\lambda) \cdot \tau(\lambda) d\lambda \quad (2)$$

where $S(\lambda)$ is the response function of the sensor on the satellite (it is sensitive only to the radiation flux in a narrow band of wavelengths), and of the transmittance of the atmosphere $\tau(\lambda)$, both terms are known from the technical specifications of the sensor and the vertical profile of the standard atmosphere (ESA, 2015), so we can determine a spatially variable flow of reflected radiation from the surface $\Phi_{reflected}$. Only a small part of the radiation flow reaches the satellite sensor, the one under the spatial angle Ω (Fig. 4) which changes due to the reflection angle Θ.

Radiant intensity $I(\lambda)$ is calculated from the radiation flux (Campbell et al., 2022) in physical units of watt / steradian.

$$I(\lambda) = \frac{d\Phi(\lambda)}{d\Omega} \quad (3)$$

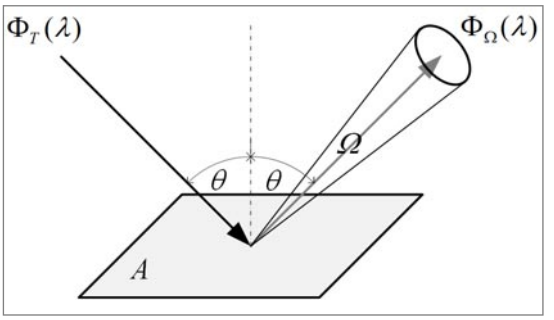

Figure 4. Relationships between the total radiation flow Φ_T and the part of the reflected short-wave radiation received by the sensor at the spatial angle Ω from the surface A, in the case of some of the channels of the multispectral sensor used in this work (MSI – MultiSpectral Instrument) wavelengths λ are large and the corresponding energy of the radiation is small, the radiation flux $\Phi_\Omega(\lambda)$ is so weak that the area A must be increased (loss of spatial resolution as a consequence) in order for sufficient radiation flux to reach the sensor for accurate measurement.

Slika 4. Odnosi ukupnog toka zračenja Φ_T i dijela reflektiranog kratkovalnog zračenja koji prima senzor pod prostornim kutom Ω s površine A, u slučaju nekih kanala multispektralnog senzora upotrebljenog u ovom radu (MSI – MultiSpectral Instrument) valne duljine λ su velike i odgovarajuća energija zračenja je mala, tok zračenja $\Phi_\Omega(\lambda)$ je toliko slab da se mora povećati površina A (što prouzročuje gubitak prostorne razlučivosti) kako bi na senzor došao dovoljan tok zračenja za precizno mjerenje.

From the radiant intensity and the known pixel area on the surface (dA, which is in this paper 10x10 m, except in the shortwave infra-red channel which has resolution of 20x20 m), the spectral radiance is calculated $L(\lambda)$, radiant flux in spectral band per unit solid angle leaving a distant source in a given direction per unit projected area in that direction (Campbell et al., 2022), Fig. 4)

$$L(\lambda) = \frac{dI(\lambda)}{dA}\cos\theta \quad (4)$$

which is measured in [watt/(steradian m^2)]. The difference in the spectral radiances will be the basis for calculating the surface burning ratio.

2.2. Spectral response differences

It is possible to distinguish healthy vegetation from burned areas due to unique reflected radiances from their surfaces, which is a consequence of the difference in their physical properties (Atun et al., 2020). Healthy vegetation reflects significantly in the green visible band (that's why we see vegetation as green) and even more strongly in the near-infrared band which is invisible to the human eye. Unlike healthy vegetation, burnt areas reflect poorly in the visible part of the spectrum (we see it as a dark, almost black surface), reflect poorly in the near-infrared region of the spectrum, but reflect more strongly in the short-wave infrared region (Fig. 5). The best distinction between vegetation and burned areas will be achieved where the average differences in reflectance are greatest, which is in the green region of the visible spectrum (around a wavelength of 0.56 μm) in the near-infrared region of the spectrum (in the range from 0.5 μm to 1.1 μm) and in the short-wave infrared region, especially at wavelengths where reflection from vegetation is weak due to absorption by water molecules in healthy vegetation. For this reason, three channels of the MultiSpectral Instrument (MSI) on the Sentinel-2 satellite were used in this paper, in which the spectral responses have the largest differences in reflectance from vegetation compared to burned areas. These are channels B3 (green visible region), B8 (near-infrared region) and B12 (short-wave infrared region). Over each of the three bands the atmosphere is transparent, and the sensors on the satellite have the highest spatial resolution of 10x10 m (the exception is channel B12, with spatial resolution of 20x20 m which is artificially resampled to the highest resolution of 10x10 m to participate equally in the following algorithms of image algebra). Technically speaking, the spectral bands of the sensor are determined by the spectral response function, which is approximately a rectangular function $S(\lambda)$ and has a determined upper and lower limit of the band (Tab. 1). A channel is usually referred to by its centre wavelength λ_C which is related to the response function, different for each channel (ESA, 2015).

$$\lambda_C = \frac{\int \lambda S(\lambda) d\lambda}{\int S(\lambda) d\lambda} \tag{5}$$

The central wavelengths and spectral widths of the used channels are shown in Table 1, the paper used a successive pair of satellite images from the Sentinel-2B satellite, the technical characteristics of the sensors of the other satellite in this two-satellite constellation (not used in this work); Sentinel-2A are almost identical. Due to the lower spatial resolution of the channel B12, it was resampled from the original spatial resolution of 20 m to a resolution of 10 m so that it could be used in algorithms of the image algebra. To conduct this, four pixels with a resolution of 10x10 m were created from a single original pixel of dimensions 20x20 m without a real increase in its spatial resolution.

Table 1. Central wavelengths used in Equation 5, band widths and spatial resolution of channels used in this work (Green – green visible, NIR – near InfraRed, SWIR – Short Wave InfraRed) (ESA, 2015).

Tablica 1. Središnje valne duljine iz jednadžbe 5, širine kanala i prostorne rezolucije primijenjene u ovom radu (Green – vidljivo zeleno područje spektra, NIR – blisko infracrveno područje, SWIR – kratkovalno infracrveno područje) (ESA, 2015).

Sentinel-2 bands	Sentinel-2A		Sentinel-2B		Both satellites
	Central wavelength (nm)	Bandwidth (nm)	Central wavelength (nm)	Bandwidth (nm)	Spatial resolution (m)
B3 – Green	559.8	36	559.0	36	10
B8 – NIR	832.8	106	832.9	106	10
B12 – SWIR	2202.4	175	2185.7	185	20

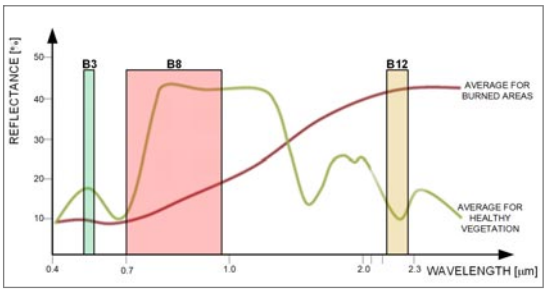

Figure 5. There are 13 available spectral bands (channels) of the MSI sensor on the Sentinel-2 satellite, in this work we used three (B3, B8 and B12) corresponded to the greatest differences in spectral response functions between average healthy vegetation and average burned areas (spectral response functions based on the function in work of Candra, 2020).

Slika 5. Ukupno je raspoloživo 13 spektralnih pojaseva (kanala) MSI senzora na satelitu Sentinel-2, u ovom radu koristili smo se trima (B3, B8 i B12) koji su odgovarali najvećim razlikama u funkcijama spektralnog odziva između prosječne zdrave vegetacije i prosječnog opožarenog područja (funkcija refleksije u ovisnosti o valnoj duljini reflektiranog zračenja preuzeta je iz rada Candra, 2020).

2.3. EFFIS methodology

Works concerning indexing of the terrain burning level mostly start from the spectral response function (Fig. 5) trying to explore the meaning of the largest detected differences between spectral response functions of the recorded spectral responses of the different channels on a satellite (Llorens et al., 2021; Kovacs, 2019). In the case of the MSI on the Sentinel-2 satellite, combinations of B3 and B8 or B8 and B12 are available, where the difference in reflectance between channels B8 and B12 is the largest, but with a minor technical difficulty as the spatial resolution of channel B12 is lower, and it is necessary to resample both channels to the spatial resolution 10 m in order to carry out further algebra of recordings (ESA, 2015).

Using channel B8 (near infrared band, NIR) and channel B12 (short wave infrared band, resampled to a spatial resolution of 10 m, SWIR) the normalized burn ratio (NBR) is calculated according to a ratio that is not

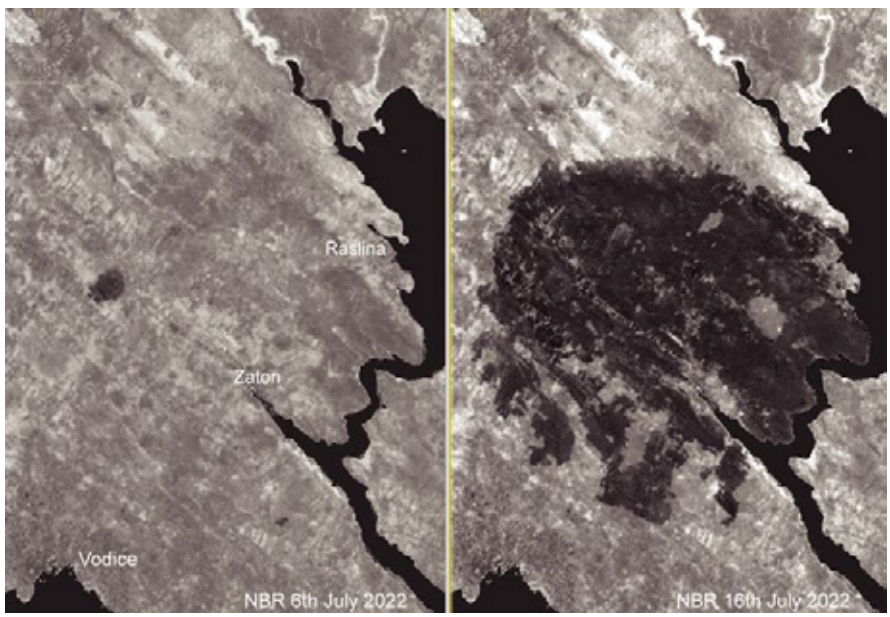

Figure 6. Normalized burn ratio (NBR) calculated by the Equation 6, on the left image is the situation before the fire occurred on July 14, 2022, and on the right image is the situation after the fire, burned areas are shown as darker areas on land, water bodies are excluded from calculation.

Slika 6. Normalizirani omjer opožarenosti (NBR) izračunat jednadžbom 6, na lijevoj slici stanje je prije požara koji se dogodio 14. srpnja 2022., a na desnoj slici stanje je nakon požara; opožarena područja prikazana su kao tamnija područja na kopnu, vodene su površine isključene.

unique only to the observed image, but can be compared with any other image (Verhegghen et al., 2016; Al-Hasn and Almuhammad, 2022):

$$NBR = \frac{NIR - SWIR}{NIR + SWIR} \quad (6)$$

where *NIR* and *SWIR* are the particular amounts of spectral radiance calculated from Equations 1 to 4. Figure 6 shows the result of Equation 6, the specific change in the normalized burn ratio as a result of a large forest fire on July 14, 2022. Pixels that are correspondent to water surfaces near Vodice, Šibenik Canal and Prokljan Lake on the right side of both images are excluded from calculation 6 as they will have influence on the distribution of NBR values, which we will discuss below (Fig. 7).

Burned and unburned areas are distinctively different in the NBR products (Fig. 6), burned areas have a significantly smaller pixel value. Using an image taken immediately after forest fire (right frame of the Fig. 6) and analyzing its histogram, a distinctive bi-modal distribution appears where the left mode represents burned areas while the right mode represents the distribution of NBR from unburned areas. In the particular satellite images, the burned mode has a maximum at NBR = -0.28, and the unburned mode has a maximum at NBR = 0.05, the minimum between them lies at NBR = -0.12.

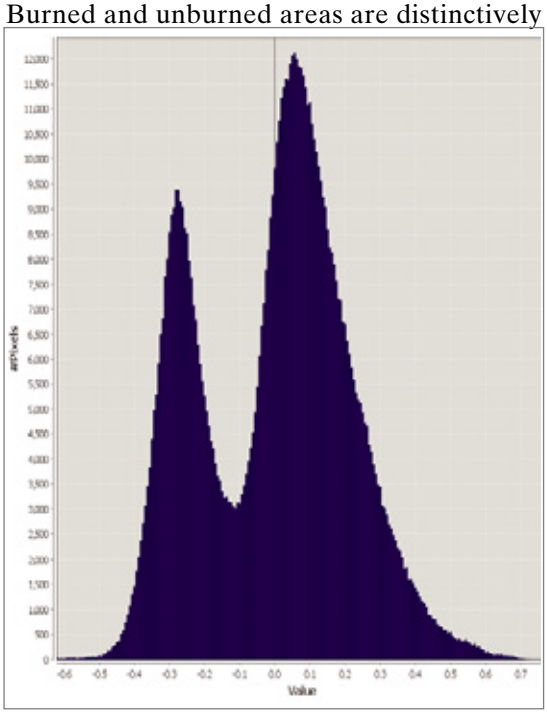

Figure 7. Normalized burn ratio (NBR) distribution histogram for the image after the fire (Fig. 6 on the right) shows how by applying Equation 6 it is possible to well distinguish between burned and unburned areas.

Slika 7. Histogram razdiobe normaliziranog omjera opožarenosti (NBR) za snimku nakon požara (sl. 6 desno) pokazuje kako se primjenom jednadžbe 6 može dobro definirati razlika opožarenog i neopožarenog područja.

From successive satellite images, with NBR calculated on both, delta Normalized Burn Ratio (*dNBR*) is derived as the difference of NBR before and after the fire (Atun et al., 2020):

$$dNBR = NBR_{before\ fire} - NBR_{after\ fire} \quad (7)$$

However, the NBR difference in Equation 7 has bias which produces too small amounts on surfaces with sparse vegetation before the fire, as is the case on the Dalmatian karst studied in this paper. For this reason, it is advisable to relativize dNBR to compute Relativized Burn Ratio (*RBR*) in the following way (Parks, Dillon and Miller, 2014):
The Relativized Burn Ratio calculated

$$RBR = \frac{dNBR}{NBR_{before\ fire} + 1.001} = \frac{NBR_{before\ fire} - NBR_{after\ fire}}{NBR_{before\ fire} + 1.001} \quad (8)$$

according to Equation 8 and rescaled to four burn categories (Tab. 2) according to the EFFIS methodology (EFFIS, 2018) is shown in Figure 8.

Table 2. Relativized Burn Ratio categories.

Tablica 2. Kategorije relativiziranog omjera opožarenosti.

Category	RBR Value	Colour
LOW	RBR < 0.26	
MODERATE	0.26 ≤ RBR < 0.42	
HIGH	0.42 ≤ RBR < 0.66	
VERY HIGH	RBR ≥ 0.66	

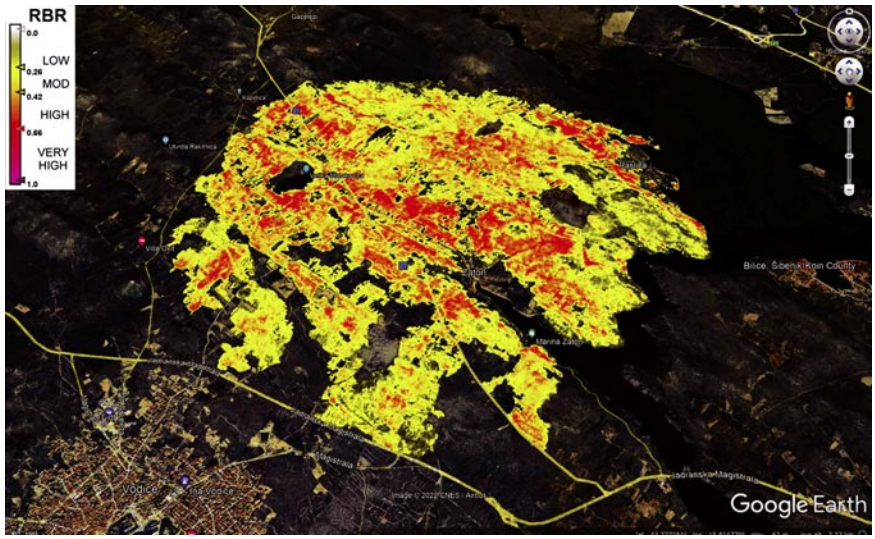

Figure 8. Categories of the Relativized Burn Ratio (RBR) as the consequence of the forest fire of 14th July 2022 near Vodice town, Croatia, standard EFFIS methodology was used.

Slika 8. Kategorije relativiziranog omjera opožarenosti kao posljedica šumskog požara 14. srpnja 2022. kraj Vodica, Hrvatska; primijenjena je standardna EFFIS metodologija.

3. RESULTS AND DISCUSSION

3.1. bi-Normalized Burn Ratio (bNBR)

Instead of direct application of the EFFIS methodology for calculating the Relativized Burn Ratio (RBR), as shown in the Chapter 2.3, we suggest modifying Equation 6 in such a way to add into account the differences in radiance between the visible, green part of the spectrum (band B3, in this case) and the radiance in the near-infrared part of the spectrum (band B8). With that taken into account, we have the new ratio of two differences in spectral radiances between three bands (sensor channels), which justifies the name of the method as "bi-Normalized Burn Ratio, bNBR".

Before that, we will show the justification of the introduction of the third band through the increase of the coefficient of variation (CV = standard deviation / mean value) for the normalized burn ratios in the case of using two channels B8 and B12 and three channels B3, B8 and B12. CV was calculated for the post-

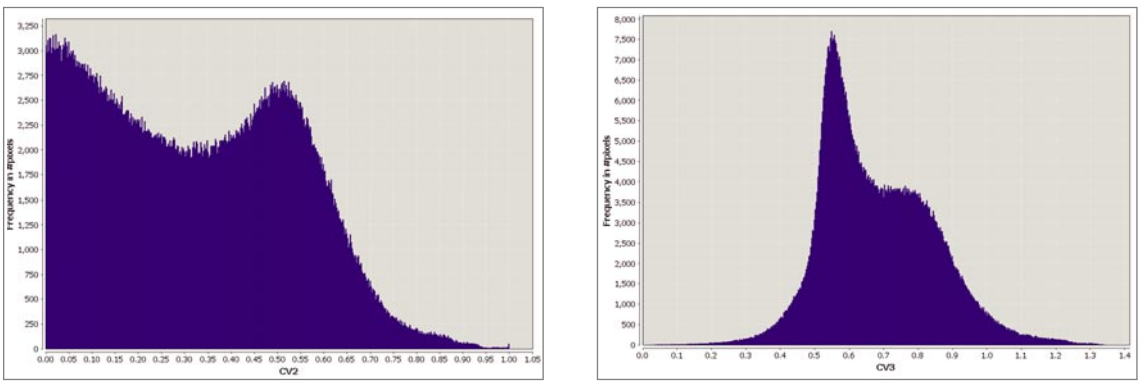

Figure 9. Differences in the coefficient of variation distribution for two channels (left, B8 and B12) and for three channels (right, B3, B8 and B12), both distributions are bimodal with the fact that in both we have the left maximum, with lower CV values, characteristic of unburned areas in a post-fire image taken on July 16, 2022.

Slika 9. Razlike razdiobe koeficijenta varijacije za dva kanala (lijevo, B8 i B12) i za tri kanala (desno, B3, B8 i B12), obje su razdiobe bimodalne s tim da je u obje lijevi maksimum, s nižim vrijednostima CV–a, karakterističan za neopožarena područja na snimci nakon požara, napravljenoj 16. srpnja 2022.

fire satellite image only, the image taken two days after the fire. Results are shown in Figure 9; on the left we have the CV_{NBR2} distribution using bands B8 and B12, and on the right side we have CV_{NBR3} distribution using three bands, B3, B8 and B12. In both cases a bimodal distribution can be seen where the lower maximum of the CV values are produced from unburnt areas. Introducing a third channel increases the number of pixels corresponding to both categories; burned, unburned, with a noticeable increase in the number of pixels in the unburned area (right). The trade-off of this approach is reduced contrast, as the modes of the CV_{NBR3} merge more into each other in the case of the three-channel coefficient of variation (Fig. 9 right).

New difference in the spectral radiances refers to the bands in the near-infrared region (band B8) and in the green region of the visible spectrum (band B3), where the difference in radi-

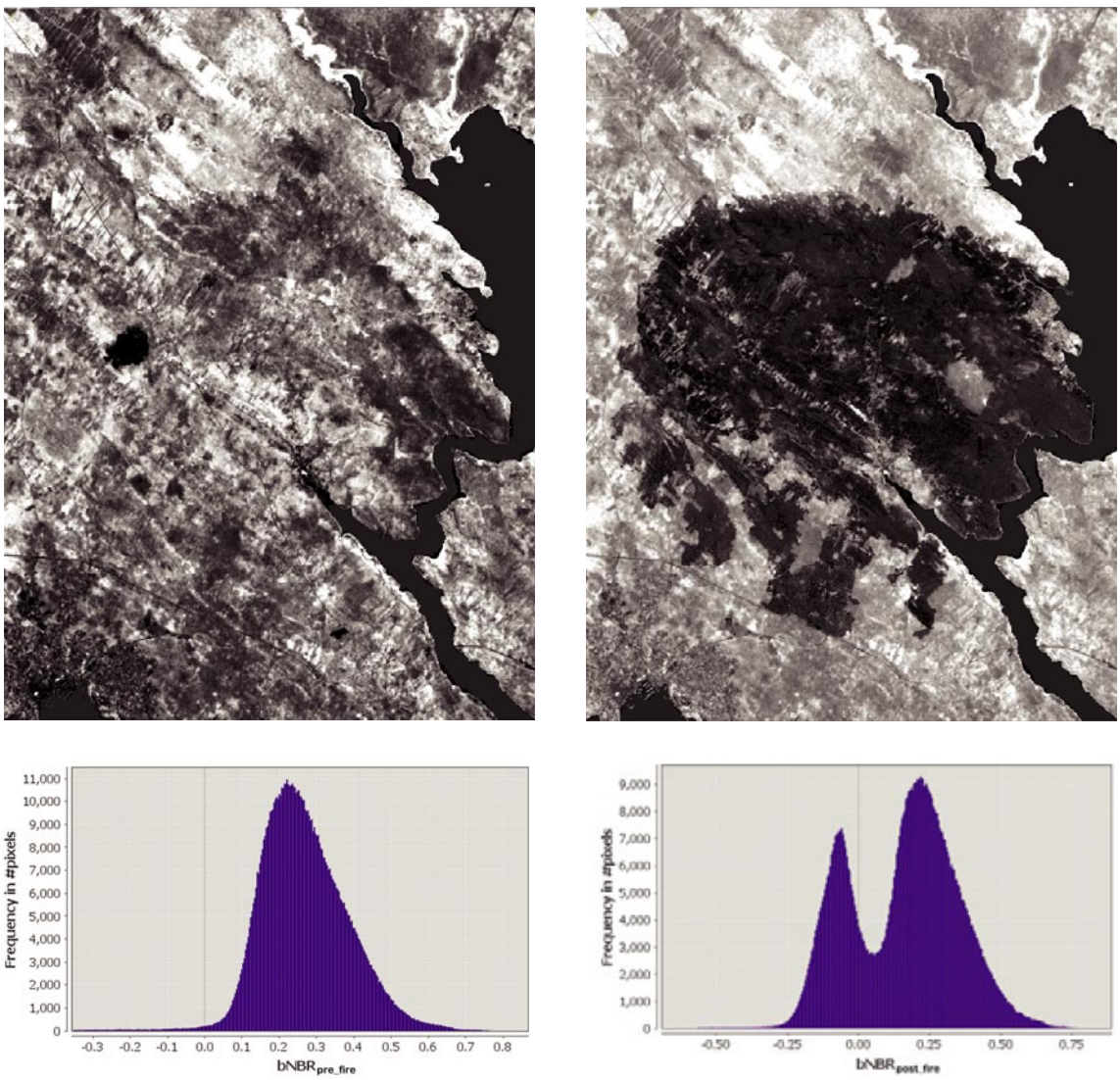

Figure 10. The difference between the bi-Normalized Burn ratio (bNBR) before (upper left) and immediately after the fire (upper right) and their corresponding histograms of the distribution of bNBR values shown below them; after the fire, a pronounced bimodal distribution appears, where the left mode belongs to the distribution from the burned areas.

Slika 10. Razlika bi-normaliziranog omjera opožarenosti (bNBR) prije (gore lijevo) i neposredno poslije požara (gore desno) i njihovi pripadajući histogrami razdioba vrijednosti bNBR-a prikazani ispod njih; nakon požara izražena je bimodalna razdioba u kojoj lijevi mod pripada razdiobi s opožarenih područja.

ances from burned and unburned areas is not as big (Fig. 5) as in the case of applying Equation 6 to channels B8 and B12 of the MSI sensor on the Sentinel-2 satellite, but due to the pronounced maxima of the spectral radiance of healthy vegetation, which is indirectly confirmed by the CV distribution histograms in Figure 9, there is justification for the proposal to introduce a new ratio, the bi-Normalized Burn Ratio (*bNBR*):

$$bNBR = \frac{NIR - SWIR + NIR - GREEN}{NIR + SWIR + NIR + GREEN} = \frac{2NIR - SWIR - GREEN}{2NIR + SWIR + GREEN} \quad (9)$$

The result of applying Equation 9 to both images, using channels B3=GREEN, B8=NIR and B12=SWIR, is shown in Figure 10. The image before the fire (top left) has only one smaller, darker scar from the earlier fire. Water surfaces were extracted on both recordings because they would affect the calculation (6) to (8) and would influence the distributions of NBR and bNBR. There were no clouds in this clip from the MSI sensor, but they need to be extracted from the image beforehand too (MSI processed to the Level-1C has masks for water surfaces, clouds and cloud shadows that just need to be included). The image before the fire has corresponded to one modal distribution of the bNBR values shown (lower left).

The image after the fire (Fig. 10, upper right) shows the burned vegetation as a large dark area, and two modes appear on the bNBR distribution histogram (lower right image), the left one which corresponds to pixels with bNBR values for burned areas. The specific parameters of the distribution depend on the size of the subset image itself, specifically how much we have chosen to keep the ratio of burned and unburned surface on them (in both cases, these are subsets of the original MSI images from Sentinel-2 that cover a much larger area of 100x100 km), so the corresponding histograms (Fig. 10. lower left and lower right) are appropriate to be qualitatively compared only.

3.2. Differential bi-Normalized Burn Ratio (dbNBR)

The bi-Normalized Burn Ratios are shown in Figure 10 along with the associated distributions of the calculated bNBR distributions shown as histograms below the correspondent images. The bNBR histogram on the image

Figure 11. Burn categorization obtained using the difference bi-Normalized Burn Ratio (dbNBR) instead of RBR (Fig. 8), the detected burned area is identical in both cases with the expected lower categories of the burned areas (see text).

Slika 11. Kategorizacija opožarenosti dobivena primjenom razlike bi-normaliziranog omjera opožarenosti (dbNBR) umjesto RBR-a (sl. 8); detektirana opožarena površina identična je s tim što je očekivano znatno manje opožarenog područja s nižim stupnjem opožarenosti (vidi tekst).

from July 6, 2022, acquired before the fire, has a unimodal, slightly right asymmetric distribution and, on this scale, no scar from the earlier fire near the hamlet of Velika Mrdakovica is visible in the histogram (Fig. 10 left up and left down). On the other hand, the satellite image taken on July 16, 2022, a couple of days after the fire, has a distinct bimodal distribution with the left maximum of bNBR pixels, which correspond to the burned areas in the image.

From the bNBR images (Fig. 10), we calculate the differential bi-Normalized Burn Ratio (dbNBR) using the same methodology that we used in the Equation 7. Due to preservation of the information about green visible channel (B3) we have presumed that the relativization, such as Equation 8 is no longer needed. The green channel will detect healthy vegetation in unburned areas, even in the cases of sparse Mediterranean vegetation types, or be able to detect remaining vegetation in burned areas. In general, it is expected that dbNBR will have a smaller proportion of the HIGH and VERY HIGH burned categories in comparison to the RBR (Figs. 11 and 8). We could expect the highest burned categories to occur in the cases of forest fires in well-developed vegetation areas somewhere else, deep in the continent.

4. CONCLUSION

Applying differential bi-Normalized Burn Ratio (dbNBR) instead of Relativized Burn Ratio (RBR) slightly complicates this image algebra algorithm and does not put a load on the available computing resources. The first results show a better gradation of lightly burned areas and a better detection of the remaining vegetation, which ultimately reduces the surface area of higher burned categories. Histograms of the distribution of NBR (Fig. 7) and bNBR (Fig. 10) indicate a very well defined decision boundary of non-burned and burned areas, which can be a pre-processing step for machine learning methods applications that benefit from clearly separated clusters. With the acquisition of more experience in the application of dbNBR, it will be possible to authoritatively answer whether a fine tune is needed between the results of RBR and dbNBR, or with the bi-Normalized Burn Ratio, relativization of the results using Equation 8 may no longer be necessary.

REFERENCES

Al-Hasn, R. and R. Almuhammad, 2022: Burned area determination using Sentinel-2 satellite images and the impact of fire on the availability of soil nutrients in Syria. *Journal of Forest Science*, **68**, 2022 (3), 96–106.

Atun, R., K. Kalkan and Ö. Gürsoy, 2020: Determining the Forest Fire Risk with Sentinel 2 Images. *Turkish Journal of Geosciences*, **Vol.1,** Issue 1, 22–26.

Campbell, J.B., R.H. Eynne and V.A. Thomas. 2022: Introduction to Remote sensing. Sixth Edition. Guilford Press, New York, ISBN 978-1-4625-4940-5, 633 pp.

Candra, D.S., 2020: Deforestation detection using multitemporal satellite images. *IOP Conf. Ser.*: Earth Environ. Sci. 500 012037, 1–13.

European Forest Fire Information System (EFFIS), 2018: User Guide to EFFIS Applications, Version 2.3.3. https://effis-gwis-cms.s3-eu-west-1.amazonaws.com/effis/reports-and-publications/effis-related-publications/effis-userguide-23.pdf, 20 pp.

European Space Agency, 2015: Sentinel-2 User handbook. ESA Standard Document Issue 1, Rev 2, 64 pp.

Jurjević, P., D. Vuletić, J. Gračan i G. Seletković, 2009: Šumski požari u Republici Hrvatskoj. *Šumarski list*, **CXXXIII (2009)**, br. 1 – 2, 63 – 72.

Kovacs, K.D., 2019: Evaluation of Burned Areas with Sentinel-2 using SNAP: the Case of Kineta and Mati, Greece, July 2018. *Geographia Technica*, **Vol. 14**, Issue 2, 20–38.

Llorens, R. et al., 2021: A methodology to estimate forest fires burned areas and burn severity degrees using Sentinel-2 data. Application to the October 2017 fires in the Iberian Peninsula. *International Journal of Applied Earth Observations and Geoinformation*, **95**, 102243, 9 pp. https://doi.org/10.1016/j.jag.2020.102243

Parks, S.A., G.K. Dillon and C. Miller, 2014: A New Metric for Quantifying Burn Severity: The Relativized Burn Ratio. *Remote Sens.*, **6**, 1827–1844., https://doi.org/10.3390/rs6031827

San-Miguel-Ayanz, J. et al., 2020: Global Wildfire Information System – Country Profiles. Publications Office of the European Union, Luxembourg, 16 pp.

San-Miguel-Ayanz, J. et al., 2021: Advance EFFIS Report on Forest Fires in Europe, Middle East and North Africa 2020. EUR 30693 EN, Publications Office of the European Union, Luxembourg, ISBN 978-92-76-37757-9, JRC124833, 34 pp. https://doi.org/10.2760/344684

Verhegghen, A. et al., 2016: The Potential of Sentinel Satellites for Burnt Area Mapping and Monitoring in the Congo Basin Forests. *Remote Sensing*, **8**, 986–1008.

Vuković, D., 2020: Statistički pregled požarnih intervencija vatrogasnih postrojbi i Oružanih snaga Republike Hrvatske u razdoblju od 2012. do 2017. godine. Završni rad, Veleučilište u Karlovcu, Odjel sigurnosti i zaštite, Stručni studij sigurnosti i zaštite, 67 str. https://urn.nsk.hr/urn:nbn:hr:128:528368.

SADRŽAJ
CONTENTS